www.cafetinnova.org

Indexed in
Scopus Compendex and Geobase Elsevier,
Geo-Ref Information Services-USA, List B of Scientific Journals, Poland, Directory of Research Journals

ISSN 0974-5904, Volume 09, No. 05

International Journal of Earth Sciences and Engineering

October 2016, P.P.2096-2105

Change Detection of Hyperspectral Remote Sensing Images Based on Deep Belief Network

FENGHUA HUANG[1-5], CHAO XU[3-5] AND ZHANGZHI ZHU[3-5]

[1]*Postdoctoral Programme of Electronic Science and Technology, Fuzhou University, Fuzhou 350116, China*
[2]*Yango College, Fuzhou 350015, China*
[3]*Key Lab of Spatial Data Mining & Information Sharing of Ministry of Education, Fuzhou University, Fuzhou 350002, China*
[4]*National Engineering Research Centre of Geospatial Information Technology, Fuzhou University, Fuzhou 350002, China*
[5]*Spatial Information Engineering Research Centre of Fujian Province, Fuzhou University, Fuzhou 350002, China*
Email: *fenghuait@sina.com*

Abstract: To address the performance bottlenecks of existing methods for change detection of hyperspectral remote sensing (HSRS) images, a new scheme for change detection of HSRS based on deep belief network (CDHSRS-DBN) is proposed. First, the HSRS images collected at two different phases (dual-temporal HSRS images) are pre-processed and registered, and then the spectral-difference images of the dual-temporal images are computed. Next, the endmember spectrums and the abundance-difference images are extracted using the pixel unmixing method based on independent component analysis (ICA). The low-layer feature vector of deep learning in CDHSRS-DBN adopts the integrated feature vector that consists of the pixel spectral-difference vector, endmember abundance-difference vector and the pixel spectral feature angle vector. Finally, a deep belief network (DBN) model that contains multi-layer restricted Boltzmann machines (RBM) and a support vector machine (SVM) is devised, and the weights of connections between visible and hidden layers are adjusted through pre-training. The accuracy of change detection is further improved by fine-tuning all the weights via the SVM classifier. In order to evaluate the performance of the proposed CDHSRS-DBN method, four pairs of EO-1 Hyperion test images at different phases, which collected in four different experimental zones, are used as the test data and CDHSRS-DBN is compared with six other typical HSRS change detection algorithms (CDHSRS-SCD, CDHSRS-MPD, CDHSRS-ICA, IR-MAD, CD-PCA and PCCD). The experiments focus on the detection of land-use changes. The average recall and precision reach 90.39% and 87.10%, respectively. The average value of F-Score and time consumption is 0.8871 and 242.5, respectively. Experimental results demonstrate the better performance of CDHSRS-DBN to detect changes of multi-temporal HSRS images accurately and efficiently.

Keywords: *Hyperspectral Remote Sensing Images, Change Detection, Deep Belief Network, Pixel Unmixing, Restricted Boltzmann Machines*

1. Introduction

Detecting changes in remote sensing images refers to automatic determination and analysis of changes that occur in ground objects by using remote sensing images collected at different phases in the same region. These changes in ground objects include variations of spectral features and spatial features [1-4]. HSRS images have hundreds, even thousands, of continuous and narrow wave bands, and they are very helpful in recognizing details of ground objects. Multi-temporal, high-dimensional spectral information can reveal changes that cannot be detected by multi-spectral data. In this context, it is very significant to detect changes of ground objects by fully exploiting multi-temporal, hyperspectral images. However, hyperspectral data is usually high-dimensional, non-linear and has many mixed pixels. Hence, automatic change detection of HSRS is not only the important academic frontier in remote sensing applications research, but also a complicated machine learning issue that needs to be further explored [4].

Currently, there have been many researches on the change detection of HSRS images across the world. Traditional methods for HSRS change detection relies on the classical single-band or multi-spectral change detection theories. Their performance in HSRS change detection is limited. Typical examples of the traditional methods for HSRS change detection include the linear transform-based change detection method [1-8], post-classification change detection method [9], abnormal change detection method [10-11], and analysis-based change detection method [12-13]. Most of existing change detection algorithms rely on linear transform, such as the Principal Component Analysis (PCA) method [2-4], the Multivariate

#02090536 Copyright ©2016 CAFET-INNOVA TECHNICAL SOCIETY. All rights reserved.

Alteration Detection (MAD) method [5], the Iteratively Reweighed MAD (IR-MAD) method [6], the Covariance Equation (CE) method [7] and the ChronoChrome (CC) method [8], et al. Currently, the used learning algorithm based on linear transform is unsupervised, and it is difficult to choose appropriate thresholds. Moreover, it cannot guarantee the discrimination performance of the obtained linear sub-space [1-8]. The post-class detection method can make full use of the information in each image and eliminates the need to consider external differences between two images, but the classification error of any image affects the detection accuracy and is prone to be accumulated [9]. In the abnormal change detection method, the focus is on detecting anomalies in difference or ratio images, and it is very effective in detecting tiny changes in images [10,11]. The analysis-based change detection method can make full use of the hyperspectral change vector to analyze the difference image and detect different types of changes; but it ignores the relationship between the spectrums of ground objects before and after changes which occur to the HSRS images. Thus, it cannot accurately analyze the changes of a single ground object over time [12-13]. To sum up, the traditional detection methods are inaccurate. To address this problem, some new change detection algorithms of HSRS images have been developed worldwide, such as those based on Tensor Factorization [14], Orthogonal Subspace Mapping [15], multi-source object feature support [16], pixel unmixing [17] and ICA [18]. These algorithms achieve improvement in detection accuracy. However, some of these novel methods only focus on one aspect of the problem and fail to provide a complete and systematic solution, or merely adopt the shallow-structure machine learning algorithms like SVM and back propagation (BP) neural network. The limitations of these methods lie in their low ability to represent complicated functions when there are a limited number of samples and computing units. Its limited generalization ability in the face of complicated classification and change detection problems becomes the bottleneck for accurate and efficient change detection in HSRS images.

Deep learning is emerging in recent years as a new method to address the limitations above. As a new research focus on machine learning, deep learning is very capable of representing functions by simulating the multi-layer operation of the human brain. In deep learning, low-layer features are combined to form more abstract high-layer representations, property types or features, and to yield the layered feature representation of the data. In this way, it can obtain more fundamental features of the input data [19]. Compared with the shallow-structure network, the deep network structure which consists of multiple non-linear mapping layers can represent complicated functions and classify complicated classes more effectively and efficiently [20, 21]. In deep learning, the multi-layer structure is used to implement unsupervised learning of different types of features in different layer respectively. The deep neural network combines the advantages of supervised and unsupervised learning to learn high-dimensional data sets more effectively. The deep learning concept is emerging as a promising solution to HSRS change detection. It is of great theoretical significance to study this issue as it has great potential of being used in various applications. DBN is a widely used and extensively studied deep learning model. Due to its ability to classify high-dimensional data more effectively by combining advantages of supervised and unsupervised learning, it has been successfully applied to automatic labeling of remote sensing images [22], classification of scenarios in high-resolution aerial images [23], recognition of small images, natural language machine learning [25], classification of remote sensing images with high spatial resolution [26], face recognition [27], HSRS image classification [28] and so on.

To eliminate the performance bottleneck of existing HSRS change detection methods, this paper proposes a DBN-based HSRS images change detection scheme called CDHSRS-DBN. First, linear pixel unmixing is done to obtain the abundance maps of each endmember and the abundance vector of each pixel in multi-temporal HSRS images. The endmember abundance-difference image of multi-temporal HSRS images is calculated. Next, a deep belief neural network which contains multi-layer RBM is designed, and the weights of connections between visible and hidden layers are adjusted through pre-training. Finally, the traditional BP network is replaced with SVM, and the parameters of CDHSRS-DBN are fine-tuned and globally optimized using a few labeled samples. In this way, the changes detection of HSRS images can be performed more accurately, efficiently and automatically.

2. SVM-based Deep Belief Neural Network (DBN-SVM)

2.1. Principle of DBN-SVM

DBN is a typical deep learning network model proposed by G. E. Hinton [29] in 2006. The traditional DBN model usually consists of a multi-layer unsupervised RBM network and a supervised single-layer BP neural network. In DBN, the RBM at each layer is pre-trained layer by layer; the output of the hidden layer of the low-layer RBM is regarded as input to the visible layer of the high-level RBM. At the fine-tuning stage, the BP network is trained through supervised learning. The error between the actual output and the expected output is back-propagated layer by layer in order to fine-tune all of the weights of the DBN [22, 23]. DBN is a probability-generating model that consists of multiple layers of RBN. Original parameters between two neighboring RBM layers are learned layer by layer

using the greedy algorithm. The training process of the RBM network can actually be regarded as initialization of weights of the BP network. This provides a solution to the problem of DBN where the BP network is prone to be stuck in local optimization and have a long training time due to random initialization of weights in the BP network [24].

Because the features of HSRS images have a high dimensionality (i.e., the number of wave bands) and it is challenging to obtain labeled samples, substituting SVM for the traditional BP algorithm can effectively avoid the dimensionality curse and local optimization, improve the global optimization efficiency of DBN parameters and enhance the training convergence speed. Hence, we implement supervised learning by substituting SVM for the traditional BP algorithm and globally fine-tune DBN. The structure of the SVM-based deep belief network is shown in Figure 1.

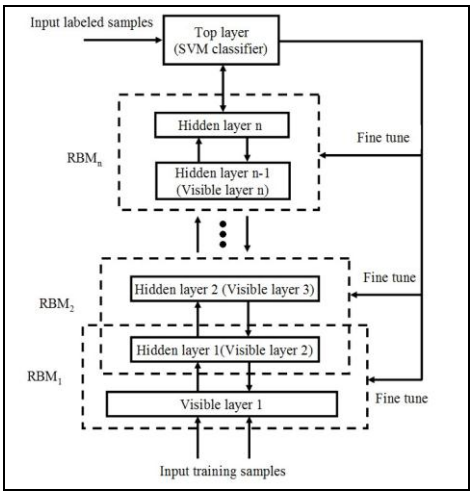

Figure1: *Structure of the DBN-SVM model*

2.2. The structure of RBM

The RBM in each layer of DBN-SVM consists of two sublayers: the hidden and the visible. The visible sublayer is mainly responsible for sample inputting and filtering, while the hidden sublayer is designed to perform data processing, analysis and output. There are two-direction connections between the elements in the hidden sublayer and the elements in the visible sublayer. However, there is no connection between elements in the same sublayer in order to enable parallel processing. The structure of the RBM in DBN-SVM is illustrated in Figure 2 [29], where the hidden and visible layers have m and n neurons, respectively. The visible-layer vector $v=(v_1,v_2\ldots..v_n)$, the hidden-layer vector $h=(h_1,h_2\ldots.h_m)$, where v_i denotes the status of the i^{th} neuron in the visible layer, h_j denotes the status of the j^{th} neuron in the hidden layer; c_1~c_m and b_1~b_n denote the offset of neurons in the hidden and visible layers, and W_{ij} denotes the weight of connection between nodes h_i and v_j.

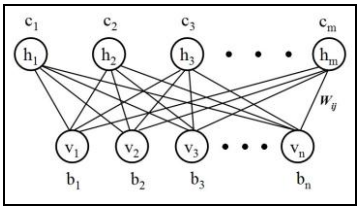

Figure 2: *The RBM structure of DBN-SVM*

The RBM of DBN-SVM is an energy-based model. Thus, the energy of RBM can be computed as Equation (2-1) [26]:

$$E(v,h) = -b'v - c'h - h'Wv \tag{2-1}$$

Based on this energy function, we obtain the joint probability distribution of (v,h), $P(v,h)$, as shown in Equations (2-2) and (2-3)[26], where S denotes the normalized factor. In practical applications, the key to P (v,h) is to compute the activation probability of each neuron at the visible and hidden layers and to calculate the optimal values of b, c, W and other parameter vectors.

$$P(v,h) = \frac{1}{S}e^{-E(v,h)} \tag{2-2}$$

$$S = \sum_{v}\sum_{h} e^{-E(v,h)} \tag{2-3}$$

Because there is no connection between neurons in the hidden and visible layers, given the status of neurons in the hidden layer, the activated status of each neuron in the visible layer is mutually independent. Hence, the activation probability of the i^{th} neuron in the visible layer can be computed as Equation (2-4) [23]:

$$p(v_i = 1) = \frac{1}{1+e^{-(a_i + h'W)}} \tag{2-4}$$

Given the status of neurons in the visible layer, the activated status of each neuron in the hidden layer is mutually independent. Hence, the activation probability of the j^{th} neuron in the hidden layer can be computed as Equation (2-5) [23]:

$$p(h_j = 1) = \frac{1}{1+e^{-(b_j + v'W)}} \tag{2-5}$$

In the RBM of DBN-SVM, samples are trained iteratively layer after layer in order to compute b, c, W and other parameter vectors, and to fit the given training data. The parameter vectors (e.g., b, c and W) can be obtained by computing the maximal log-likelihood function of the activation probability in the training set [26]. Each parameter can be updated using the contrastive divergence (CD) algorithm proposed by Hinton in [30].

3. DBN-Based Change Detection of HSRS Images (CDHSRS-DBN)

The procedures of the proposed DBN-based method for change detection of HSRS images (CDHSRS-DBN) are shown in Figure 3. The imaging of hyperspectral sensors is subject to interference from many factors, and bias exists in most of the original HSRS images. Hence, the HSRS images need to be pre-processed first. The pre-processing methods for HSRS images include problematic wave bands elimination, radiation correction, bad line restoration, strip elimination, smile effect removal, atmosphere correction, spectral reflectivity inversion and calibration [25]. Problematic wave bands refer to the abnormal wave bands which are non-calibrated, overlapped, heavily corrupted with noise, influenced by steam or confirmed to provide little information on the ground. Moreover, the HSRS images that are captured at different phases and imaging angles have different reference systems. So, it is necessary to precede change detection with precise image registration and to make the root-mean-square (RMS) error of registration less than 0.5. After pre-processing and registration, we need to compute the spectral difference-image, unmix the pixels and extract the endmember spectrums via the ICA (independent component analysis) method which are mentioned in the literatures [18] and [31]. In this paper, ICA is done on the difference-image to obtain the independent components (endmembers) and the abundance-difference of each endmember. Finally, we obtain the endmember abundance difference-images.

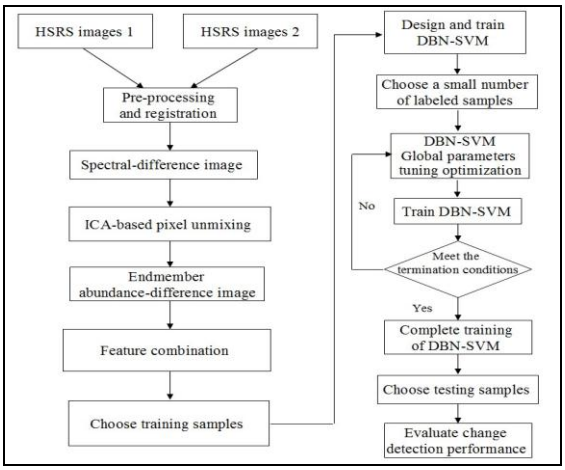

Figure 3: *Procedures of CDHSRS-DBN*

We define an integrated feature vector [δ, Δsp, θ], where δ denotes the endmember abundance change vector, Δsp denotes the continuous spectral-difference vector, and θ denotes the included angle of the spectral feature vectors in different phases. The vector [δ, Δsp, θ] is used as the low-layer feature vector of DBN deep learning. The labeled samples are extracted from field survey and relevant materials, and the DBN-SVM is constructed and pre-trained layer by layer. Then, a small number of labeled samples are input to the top-layer SVM classifier for supervised training. Feedback on the RBM at each layer is obtained using the SVM classifier to fine-tune and globally optimize the parameters of DBN-SVM until the parameters of DBN-SVM at each layer meet the requirements. Finally, the trained DBN-SVM model is used together with the non-labeled samples for performance evaluation. In CDHSRS-DBN training, the number of network layers and the number of neurons in the hidden layers have great influence on change detection. Experiments are performed in this paper to determine their optimal values.

In this work, the changed status of the pixels in HSRS images is either "changed" or "unchanged". Detection performance is evaluated using the following four metrics: P (Precision), R (Recall), F (F-Score) and T (Time Consumption). Let $N1$ denote the number of correctly detected pixels that have changed in the experimental zone, $N2$ denote the total number of detected pixels that have changed in the experimental zone, and $N3$ denote the number of pixels that have actually changed in the experimental zone. Then, the definitions of P, R and F are as Equations (3-1), (3-2) and (3-3):

$$P = N1/N2 \times 100\% \quad (3\text{-}1)$$

$$R = N1/N3 \times 100\% \quad (3\text{-}2)$$

$$F = \frac{2 \times P \times R}{P + R} \times 100\% \quad (3\text{-}3)$$

F is the harmonic mean of P and R, and it can indicate the performance of the algorithm overall by combining the two metrics. F can also alleviate contradiction between P and R. The higher the F, the better the algorithm [32]. Time consumption T reflects the efficiency of the pixel change detection and it is another important performance metric in addition to change detection accuracy.

4. Experiments and Result Analysis

4.1. Experimental zone and choice of samples

4.1.1. Basic data and pre-processing

In order to improve reliability of the research results, four EO-1 Hyperion HSRS images (Level L1G) are chosen for the experiments, and two images of them cover the same regions at different phases, and their coverage regions are located in XinYang City, Henan Province; the other two images of them also cover the same regions at different phases, but their coverage regions are located in the Changping District, Beijing City. The EO-1 Hyperion data (L1G) has 242 wave bands, including 35 visible bands, 35 near-infrared bands, and 172 shortwave infrared bands. The spectral range is 0.4～2.5μm, the spectral resolution is 10 nm, and the spatial resolution is 30m. Two representative experimental zones were chosen respectively from the two coverage regions described above (that is, four experimental zones are selected). Details of each experimental zone are listed in Table 1.

Table 1: *Basic information of experimental zones*

Names of experimental zones	Sizes of experimental zones (pixels)	Central position (rectangle)	Imaging time	Address
Zone 1	187×268	32°16'56.1875"N, 114°32'52.5174"E	2003-02-18 2005-01-14	Nearby Dalin Town and Dongpu Town in Luoshan County, Xinyang City, Henan Province
Zone 2	185×271	31°55'21.1725"N, 114°26'58.8077"E	2003-02-18 2005-01-14	Nearby Panxin Town in Luoshan County, Xinyang City, Henan Province
Zone 3	134×306	40°7'50.0400"N, 116°24'42.8152"E	2001-11-27 2003-04-07	Near Dongxiaokou Town, Changping District, Beijing
Zone 4	142×271	40°3'3.0125"N, 116°23'12.8551"E	2001-11-27 2003-04-07	Near Beiqijia Town, Changping District, Beijing

In this work, four pairs of HSRS test images corresponding to the above four experimental zones are used as the test hyperspectral data in the experiments. In addition to the EO-1 Hyperion data of images, we carried out field survey and collected historical materials to obtain a lot of data on land-use of the four experimental zones above. They constitute the most important source of samples for HSRS change detection experiments.

The first step of pre-processing EO-1 Hyperion images of experimental zones is to eliminate problematic wave bands. After elimination, each of the two groups of EO-1 Hyperion images had 152 bands, numbered 12~57, 81~119, 133~164, 183~184 and 188~220. Then, these EO-1 Hyperion images were subjected to radiation correction, bad line restoration, strip elimination, smile effect removal, atmosphere correction and geometrical registration.

4.1.2. Selection of samples

The types of land use in the four experimental zones mainly include grassland, land for construction, forest land, nudation, farm land and water body. The training and testing samples can be classified into changed and unchanged categories. After the comprehensive analysis of field investigation, corresponding historical data and other remote sensing images of the similar coverage, the changed and unchanged samples from each experimental zone are selected randomly and divided equally into two halves (one half of them are training samples, and the other half of them are testing samples). The number of the samples for each experimental zone is shown in Table 2. After extraction of relevant samples, we needed to normalize the feature data of training and testing samples in order to eliminate difference both features and metrics in terms of dimensionality, order and data dispersion.

Table 2: *Number of samples for each experimental zone*

Experimental zones	Training samples (changed)	Training samples (unchanged)	Testing samples
Zone 1	500	500	50116
Zone 2	1000	1000	50135
Zone 3	2000	2000	41004
Zone 4	3000	3000	38482

4.2. Feature extraction and combination

The HSRS images have continuous and fine-granularity wave bands and high spectral resolutions. Continuous and fine-granularity spectrums of ground objects are essential for distinguishing ground objects effectively. Therefore, in order to determine whether pixels have changed, in addition to the endmember abundance change vector $\delta = [\delta_1, \delta_2, .. \delta_p]$, we need to comprehensively consider the continuous spectral-difference vector $\Delta sp = [\Delta sp_1, \Delta sp_2, ...\Delta sp_w]$ (where w is the number of effective wave bands in the hyperspectral images after eliminating problematic wave bands), and the included angle θ of spectral feature vectors. The included angle θ can be computed as equations (4-1):

$$\theta = \arccos(a \bullet b / (|a| * |b|)) \qquad (4\text{-}1)$$

Where a and b denote the spectral vectors of the pixel at the former and latter phases, $|a|$ and $|b|$ denote the modulo of a and b, $a \bullet b$ denotes the inner product of a and b. The integrated feature vector $F = [\delta_1, \delta_2,...\delta_p, \Delta sp_1,\Delta sp_2,.....\Delta sp_w, \theta]$ is used as the low-layer feature of deep learning at DBN-SVM, with a dimensionality of 163 in total (p=10 and w=152).

4.3 Experiment on CDHSRS-DBN-based change detection

Before carrying out the experiment on CDHSRS-DBN-based change detection, a DBN-SVM network model which involves optimization of the DBN-SVM parameters needs to be constructed firstly. These parameters includes the number of RBM layers, the number of neurons in the hidden layer, the number of neurons in the input and output layers, and the number of sample iterations at the pre-training and fine-tuning stages. From the principles and structures of DBN-SVM discussed in Section two, we know that the performance of the DBN-SVM is largely dependent on these parameters. In this paper, the optimal settings

of these parameters were determined empirically and through simulation[21,24].The overall change detection accuracy reaches the highest level when each of hidden layers in DBN-SVM has the same number of neurons, the number of RBM layers (exclusive of the SVM layer) is set to 4 and the number of neurons in the hidden layer is 64. At the pre-training stage, the weight of connections between the visible and hidden layers is adjusted constantly through iteration in order for the entire network to learn the fundamental features of the input samples effectively. After construction of the deep network with four layers of RBM, the SVM classifier is used to fine-tune the weights of the DBN-SVM for the purpose of further improving the change detection accuracy. Experimental results indicate that the overall performance of DBN-SVM converges to a stable level after 1500 sample iterations at the pre-training stage and 2000 fine-tuning iterations. Moreover, the number of neurons in the input layers of the DBN-SVM (the number of neurons in the first RBM visible layer) is equal to the dimensionality of the low-layer integrated feature vector (163) in our experiment, while there is only one neuron in the output layer (SVM classifier), where the change detection result is either *changed* (1) or *unchanged* (0).

In this work, land-use change is classified into two categories: changed or unchanged. Figures 4-7 show the land-use changes detected by applying the proposed CDHSRS-DBN to the four pairs of HSRS images described above.

Although the four pairs of testing images have different levels of complexity and a few of changes suffer misdetection and omissions, CDHSRS-DBN was able to correctly detect most of the land-use changes. In the four pairs of testing images, the changes that occur to the farm land and the land for construction are prone to be misdetected or omitted. This is mainly because the types of crops grown, the growth status and the amount of water storage in the farm land vary greatly and frequently, and the regularity of reflectance spectrum from farm lands is not obvious. The land for construction differs enormously in terms of earth surface coverage, types of buildings and the materials of rooftops. Moreover, the reflected light from buildings provides serious interference, and it is challenging to unmix pixels. Hence, it is very difficult to detect changes in farm land and land for construction based on spectral changes of the reflected light. In addition, spectrum similarity exists among some forest land, farm land, grass land, wet land and paddy field, and this increases the possibility of misdetection. The performance metrics of CDHSRS-DBN for the four pairs of testing images are given in Table 3. Table 3 indicates that the average precision and average recall of CDHSRS-DBN for the four pairs of testing images are 90.39% and 87.10%, respectively; the average value of F-Score is 0.8871. This demonstrates CDHSRS-DBN can detect land use changes of multi-temporal HSRS images very accurately.

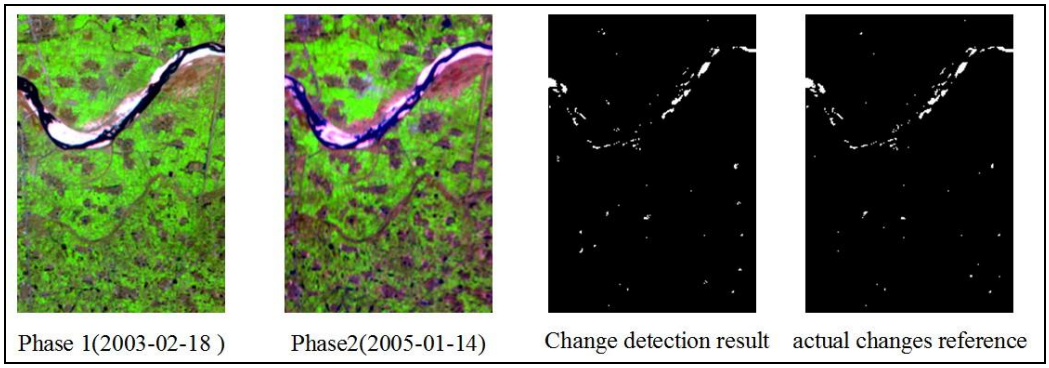

Figure 4: *Change detection results of hyperspectral images for the first experimental zone (RGB: 164/48/31)*

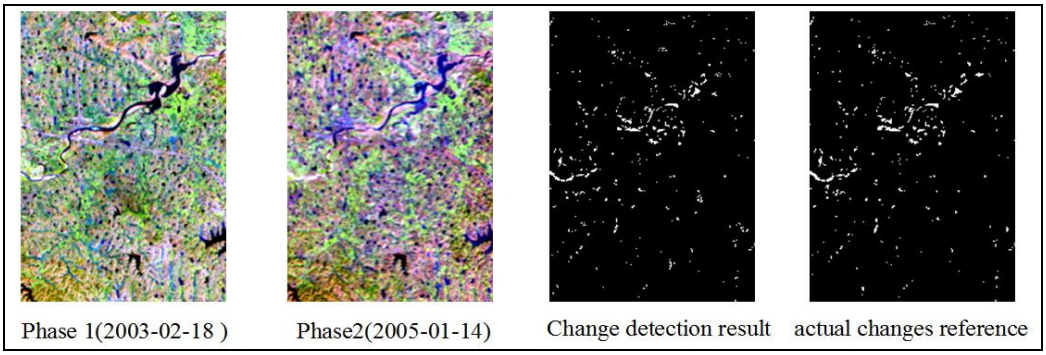

Figure5: *Change detection results of hyperspectral images for the second experimental zone (RGB: 164/48/31)*

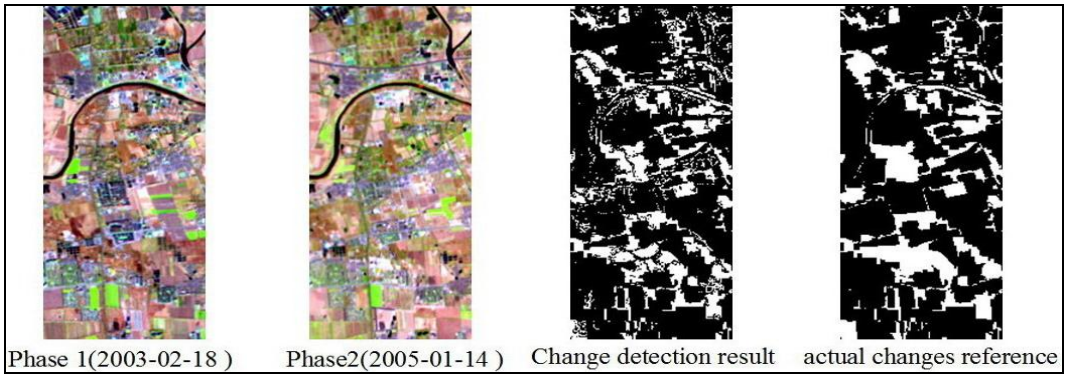

Figure 6: *Change detection results of hyperspectral images for the third experimental zone (RGB: 164/48/31)*

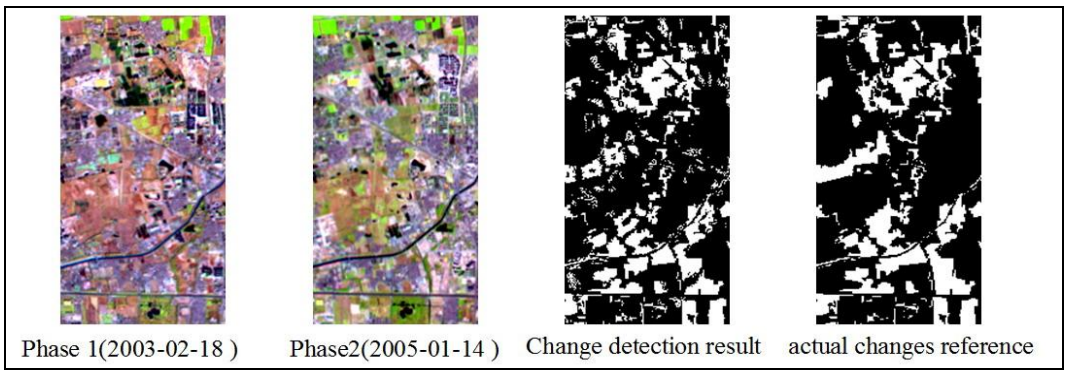

Figure7*: Change detection results of hyperspectral images for the fourth experimental zone (RGB: 164/48/31)*

Table 3: *Analysis of change detection results for each experimental zone*

Experimental zones	N1	N2	N3	Misdetections	Omissions	Precision (P/%)	Recall (R/%)	F-Score
Zone 1	475	515	549	40	74	92.23	86.52	0.8929
Zone 2	839	933	974	94	135	89.92	86.14	0.8799
Zone 3	8909	9989	10238	1080	1329	89.19	87.02	0.8809
Zone 4	8829	9785	9951	956	1122	90.23	88.72	0.8947
Averages						90.39	87.10	0.8871

4.4. Comparison of CDHSRS-DBN with other methods

In order to evaluate the performance of CDHSRS-DBN, we compared it with the post-classification

change detection method (PCCD) [11-13], principal component analysis-based change detection method (CD-PCA) [2,3,4], iterative weighting-based multi-variable change detection method (IR-MAD) [6-7], feature subspace-based hyperspectral image change detection method (CDHSRS-SCD) [22], pixel unmixing-based hyperspectral image change detection method (CDHSRS-MPD) [24-27], and the independent component analysis-based hyperspectral image change detection method (CDHSRS-ICA)[18]. In PCCD, the images collected at different phases are classified first, and the changes in ground objects are then determined based on classification results. Its detection accuracy is directly related to the classification accuracy of each image, and the error is prone to be accumulated. Hence, its change detection accuracy needs to be further improved. In CD-PCA, the difference-image undergoes PCA transformation, or the dual-temporal images are combined into a single image which is then subjected to PCA transformation. This method focuses on the difference between wave bands, and highlights the changed region by integrating information on the changes, but it is mostly suited for multi-spectral data without paying sufficient attention to the features of hyperspectral data. Thus, it is efficient but inaccurate. IR-MAD is developed by combining the traditional MAD algorithm with the expectation maximization (EM) algorithm. It detects changes in ground objects by assigning weights to pixels and altering thresholds. It is also very suited for multi-spectral data but ineffective for change detection of hyperspectral images. CDHSRS-SCD is very implementable and accurate, but its major problems lie in the inefficiency of detecting fine-granularity spectral changes and the difficulty of constructing the subspace. CDHSRS-MPD needs to first determine the dimensionality of hyperspectral data and the number of endmembers, extract pure spectral features from ground objects (endmembers), and then compute the corresponding abundance maps. Finally, it detects changes through

pixel unmixing together with the difference between abundance maps. Change detection accuracy is improved greatly. In CDHSRS-ICA, pixel unmixing is done via ICA, and skewness-based ICA is performed on the endmember-difference image. The change in single ground object is shown separately in different component figures in order to extract the changes information. This method is very efficient without increasing the rate of misdetection.

The proposed CDHSRS-DBN is compared with other six methods (CDHSRS-SCD, CDHSRS-MPD, CDHSRS-ICA, IR-MAD, CD-PCA and PCCD) using the experimental data of the four pairs of testing images in subsection 4.3. The experimental results are shown in Table 4. The algorithm performance is evaluated using the following four metrics: average prevision P_avg, average recall R_avg, average F-Score F_avg and average time consumption T_avg.

Table 4: *Comparison of experimental results for different detection algorithms*

Change detection methods	P_avg/%	R_avg/%	F_avg	T_avg/s
CDHSRS-DBN	90.39	87.10	0.8871	242.5
CDHSRS-SCD	88.07	85.86	0.8694	175.2
CDHSRS-MPD	86.60	0.8447	0.8551	165.6
CDHSRS-ICA	86.94	0.8481	0.8585	121.8
IR-MAD	85.86	0.8374	0.8478	179.5
CD-PCA	82.25	0.8022	0.8121	119.3
PCCD	80.82	0.7888	0.7983	133.9

Table 4 indicates that CDHSRS-DBN consumes more time than other methods, but it is superior in terms of average precision, average recall and average F-Score, which are 90.39%, 87.10% and 0.8871, respectively. The change detection accuracy of CDHSRS-SCD is only next to CDHSRS-DBN, but its time consumption is much less than CDHSRS-DBN. The change detection accuracy of CDHSRS-MPD is close to that of CDHSRS-ICA, and both of them are inferior to CDHSRS-SCD in terms of accuracy. But their time consumption is also less than CDHSRS-SCD. Hence, CDHSRS-SCD, CDHSRS-MPD and CDHSRS-ICA put in remarkable performance on hyperspectral change detection. But compared with CDHSRS-DBN, they cannot represent complicated functions effectively when there is a limited number of samples and computing units. Moreover, their generalization ability is poor in the face of change detection of hyperspectral images. This is why they cannot detect changes of hyperspectral images accurately. The accuracy of IR-MAD is slightly less than CDHSRS-ICA, but its time consumption is ranked second, only next to CDHSRS-DBN. This is mainly because IR-MAD assigns different weights to pixels through constant sample iteration, and determines whether changes occur to pixels based on final weights of pixels and the weighting threshold. But in the case of change detection of high-dimensional data, the number of sample iterations needed for pixel weights to converge increases dramatically, and the threshold is mostly set up manually, greatly affecting accuracy and efficiency of change detection. CD-PCA and PCCD can detect changes efficiently, but the accuracy is lower. The change detection accuracy of PCCD is lowest of all the methods above. Mixed pixels have great influence on HSRS images, the classification accuracy of single-temporal image is limited, and the errors tend to be accumulated during multi-temporal change detection. In this context, the accuracy of PCCD is very low because it is directly related to the classification accuracy of single-temporal image. In CD-PCA, subjecting the hyperspectral difference image or the combined image to PCA transformation causes heavy loss of feature information. The alleviation of high-dimensional features reduces the change detection accuracy of hyperspectral images. To sum up, the proposed CDHSRS-DBN is superior to the other methods overall.

5. Analysis and Discussion

The proposed CDHSRS-DBN focuses on checking whether a certain pixel has changed, instead of addressing the "from-to" problem for a particular type of ground object. Although the CDHSRS-DBN proposed in this paper can detect changes in HSRS images effectively, there are still some issues.

In this work, ICA is used for linear pixel unmixing. When the hyperspectral images follow or almost follow a linear model, endmembers can be extracted from mixed pixels and generate abundance maps very accurately, efficiently and automatically. But when the hyperspectral images follow a non-linear model, the endmember spectrums cannot be extracted accurately. Hence, the ICA-based pixel unmixing needs to be improved and adapted to nonlinear hyperspectral images.

In addition, the low-layer features of multi-temporal HSRS images contain spectral features, spatial features, temporal features and spatio-temporal autocorrelation features, and so on. But in this work, a integrated feature vector $F=[\delta, \Delta sp, \theta]$ is defined as the low-layer feature vector of DBN-SVM deep learning, where δ denotes the endmember abundance change vector, Δsp denotes the continuous spectral difference vector, and θ denotes the included angle of the spectral feature vector. Obviously, F is a spectral feature vector and the other features of hyperspectral images are not fully exploited. Furthermore, when the low-layer features of hyperspectral images are

described in this work, the various feature vectors are only combined simply without considering the mutually constraining relationship among feature vectors in the temporal-spatial-spectral features space. This may cause the loss of low-layer features. How to optimize the combination of low-layer features for DBN-SVM is an issue that needs to be studied in the future.

6. Conclusions

In this work, the proposed CDHSRS-DBN fully absorbs the advantages of DBN, pixel unmixing and SVM, and greatly improves change detection accuracy. CDHSRS-DBN was compared with six other typical algorithms (CDHSRS-SCD, CDHSRS-MPD, CDHSRS-ICA, IR-MAD, CD-PCA and PCCD) and the results demonstrate its superiority as its average recall, average precision, average F-Score and average time consumption are 90.39 %, 87.10 %, 0.8871 and 242.5 seconds, respectively. However, there are still some defects with our work. For example, the pixel unmixing method needs to be further improved, and the utilization and combination of low-layer features need to be further optimized. When the multi-temporal HSRS images are of poor quality or follow nonlinear model, the accuracy and efficiency of CDHSRS-DBN will be affected. In the future, we will comprehensively consider these issues and strive to propose a new method that can detect changes of HSRS images even more accurately, efficiently and automatically.

7. Acknowledgements

This work was funded by the China Postdoctoral Science Foundation Project (2015M571963), the National Natural Science Foundation of China (NSFC, 41501451), the Program for Outstanding Youth Scientific Research Talents in Fujian Province University (OYSRTFJ,2015) and the Program for New Century Excellent Talents in Fujian Province University (NCETFJ, 2016). The authors would like to thank Rui Xu and Qian Weng for their assistance, suggestions, and discussions.

References

[1] M.J.Canty and A.A.Nielsen, "Linear and kernel methods for multivariate change detection", *Computers & Geosciences*, No.38, PP.107-114, 2012.

[2] K.Wu, R.Niu,Y.Wang and B.Du,"Change Detection of Multi-spectral Remote Sensed Images Based on PCA and EM Algorithm", *Computer Science*, Vol.37, No.3,PP. 282-284+296,2010.

[3] J.S.Deng, K.Wang, Y.H.Deng and G.J.Qi, "PCA-based land-use change detection and analysis using multitemporal and multisensor satellite data", *International Journal of Remote Sensing*, Vol.29, No.16, PP.4823-4838, 2008.

[4] A.A.Nielsen, R.Larsen and J.S.Vestergaard, "Sparse Principal Component Analysis in Hyperspectral Change Detection", *SPIE Europe Remote Sensing Conference*, Prague, Czech Republic, PP.547-556, 2011.

[5] A.A.Nielsen, K.Conradsen and J.J.Simpson, "Multivariate Alteration Detection (MAD) and MAF Postprocessing in Multispectral, Bitemporal Image Data: New Approaches to Change Detection Studies", *Remote Sensing of Environment*, Vol.64, No.1, PP.1-19, 1998.

[6] P.Marpu, P.Gamba and J.A.Benediktsson, "Hyperspectral change detection using IR-MAD and feature reduction", *Proceedings of IEEE: International Geoscience and Remote Sensing Symposium (IGARSS 2011)*, Vancouver, Canada, PP.24-29, 2011.

[7] A.P.Schaum and A.Stocker, "Hyperspectral Change Detection and Supervised Matched Filtering Based on Covariance Equalization", *Proceedings of SPIE: Algorithms and Technologies for Multispectral, Hyperspectral, and Ultraspectral Imagery XV*, Orlando, Florida, USA, PP.77-99, 2004.

[8] A.Schaum and A.Stocker, "Long-interval chronochrome target detection", *Proceedings of the International Symposium on Spectral Sensing Research*, PP.1760-1770, 1998.

[9] K.Vongsy and M.J.Mendenhall, "Improved change detection through post change classification A case study using synthetic hyperspectral imagery", *IEEE: The 2nd Workshop on Hyperspectral Image and Signal Processing: Evolution in Remote Sensing (WHISPERS)*, PP.14-16, 2010.

[10] C.Wu, L.P.Zhang and B.Du, "Hyperspectral anomaly change detection with slow feature analysis", *Neurocomputing*, No.151, PP.175-187, 2015.

[11] B.Du and L.P.Zhang, "Random-selection-based anomaly detector for hyperspectral imagery", *IEEE Transactions on Geoscience and Remote Sensing*, Vol.49, No.5, PP.1578-1589, 2011.

[12] Q.Du, N.Younan and R.King, "Change Analysis for Hyperspectral Imagery", *International Workshop on Analysis of Multi-temporal Remote Sensing Images*, PP.1-4, 2007.

[13] D.Lu, P.Mausel, E.Brondízio and E.Moran, "Change detection techniques",*International Journal of Remote Sensing*, Vol.25,No.12,PP.2365-2407,2004.

[14] Q.Du, "A new method for change analysis of multi-temporal hyperspectral images", *Workshop on Hyperspectral Image & Signal Processing (WHISPERS): Evolution in Remote Sensing*, PP.1-4, 2012.

[15] C.Wu,B.Du and L.P.Zhang, "A Subspace-Based Change Detection Method for Hyperspectral Images", *IEEE Journal of Selected Topics in*

Applied Earth Observations and Remote Sensing, Vol.6,No.2,PP.815-830,2013.

[16] B.T.Jiang, B.Fan and X.L.Zhang, "A Novel change Detection Method for Hyperspectral Images Based on Multisource Target Feature Support", China Patent (201210247785.3), 2012.

[17] A.Ertürk and A.Plaza, "Informative Change Detection for Hyperspectral Images by Unmixing", *IEEE Geoscience and Remote Sensing Letters*, Vol.12, No.6, PP.1-5, 2015.

[18] C.Wu, B.Du and L.P.Zhang, "Hyperspectral change detection based on independent component analysis", *Journal of Remote Sensing*, Vol.16,No.3,PP. 545-561, 2012.

[19] B.Yin, W.Wang and L.Wang, "Review of Deep Learning", *Journal of Beijing University of Technology*, Vol.41, No.1, PP.48-59, 2015.

[20] Z.Sun, L.Xue, Y.Xu and Z.Wang, "Overview of deep learning", *Application Research of Computers*, Vol.29, No.8,PP. 2806-2810, 2012.

[21] J.Schmidhuber, "Deep learning in neural networks: An overview", Neural *Networks*, No.61, PP.85-117, 2015.

[22] H.J.Chen, M.L.Huang, L.Jiang and J.H.Tao, "A Deep Learning-Based Method for Automatic Labelling of Remote Sensing Images", China Patent (201410039584. 3), 2014.

[23] X.L.Li, Z.X.Zhang, Y.H.Wang and Q.J.Liu, "Aerial Images Categorization with Deep Learning", *Journal of Frontiers of Computer Science & Technology*, Vol.8, No.3, PP.305-312, 2014.

[24] G.Lu, P.Hao and J.L.Sheng, "On Applying an improved Deep Neural Networks in Tiny Image Classification", *Computer Applications and Software*, Vol.31, No.4, PP.182-184+213, 2014.

[25] S.S.Zhou, Q.C.Chen and X.L.Wang, "Active deep learning method for semi-supervised sentiment classification", *Neurocomputing*, Vol.120, No.10, PP. 536-546, 2013.

[26] Q.Lv,Y.Dou and X.Niu, "Remote Sensing Image Classification Based on DBN Model", *Journal of Computer Research and Development*, Vol.51,No.9,PP. 1911-1918,2014.

[27] R.M.Chai and Z.J.Cao, "Face Recognition Algorithm Based on Gabor Wavelet and Deep Belief Networks", *Journal of Computer Applications*, Vol.34, No.9, PP.2590-2594, 2014.

[28] Y.S.Chen, X.Zhao and Q.Wang, "A Deep Learning Based Method for Classification of Hyperspectral Remote Sensing Data", China Patent, (201410359935.9), 2014.

[29] G.E.Hinton, S.Osindero and Y.W.Teh, "A fast learning algorithm for deep belief nets", *Neural Computation*, Vol.18, No.7, PP.1527-1554, 2006.

[30] G.E.Hinton, "Training products of experts by minimizing contrastive divergence", Neural Computation, Vol.14, No.8, PP. 1771-1800, 2002.

[31] J.Wang and C.I.Chang, "Applications of independent component analysis in end member extraction and abundance quantification for hyperspectral imagery", *IEEE Transactions on Geoscience and Remote Sensing*, Vol.44, No.9, PP. 2601-2616, 2006.

[32] A.O.Ok, "Automated Detection of Buildings from Single VHR Multispectral Images Using Shadow Information and Graph Cuts", *ISPRS Journal of Photogrammetry and Remote Sensing*, Vol. 86, No.12, PP. 21-40, 2013.